Validation of MAPS: a novel 6-degree-of-freedom position sensor for nanopositioning

Richard Aras[1], James Dallas[1], Edward Heaps[2], László Varga[3], and Andrew Yacoot[2]

[1] Anemos Technology Ltd, 100 Fenchurch Street, London, EC3M 5JD, UK.

[2] National Physical Laboratory, Hampton Road, Teddington, Middlesex, TW11 0LW UK.

[3] Anemos and University of Szeged, H-6720, Szeged, Árpád Sq. 2, Hungary.

Abstract

Anemos' multi-dimensional absolute position sensors (MAPS) consists of a photolithographically defined reference scale, a camera, and computer image processing that decodes relative position of a camera to the scale. A series of experiments tested the novel opto-electronic sensor against traceable National Physical Laboratory (NPL) optical interferometers (OI) with motion provided by nanopositioning stages. Initially, MAPS to OI agreement was verified to be within 5 nm in the lateral (XY) axes across 100 µm travel. However, when MAPS, OI, and stage position were correlated across much finer steps, MAPS demonstrated repeatability and noise below 100 pm, indicating that the larger discrepancies seen previously were due to Abbe effects, servo-mechanical, and other OI/MAPS-extrinsic factors. In a third experiment, the outputs of four orthogonally placed MAPS 6DoF sensors were correlated against each other, OI, and feedback from a single-axis stage. Here, MAPS displayed sub-nanometre agreement with other sensors, and consistency across independent MAPS sensors. A fourth experiment collected millions of MAPS sample points during repetitive 1 nm circular motion. Spectral analysis of these large datasets, correlations between noise in multiple axes and repeatability indicate MAPS may resolve single digit picometre movements. These results corroborate simulations and supports the feasibly of million-to-one position interpolation from the MAPS 5 µm-grid reference scale. This equates to an unprecedented 40-bit dynamic range since MAPS can sustain measurement resolution over metres of travel. Overall, the experimental series highlight the challenges of nanoscale calibration and benefit of full 6DoF sensing in real-world nano-positioning systems.

Keywords: metrology, 3D measurements, interferometer, position sensor.

Introduction

Multi-axis motion and associated dimensional metrology are critical across all length scales [1,2] in industries such as robotics, CNC machining, wafer-steppers, and nanotechnology. Three-dimensional positioning systems, irrespective of the working length, have at least 21 sources of error [3,4], and considerable effort has been directed towards characterising them, particularly to support coordinate measuring systems.

Typically, motion control systems constrain movements to a single degree of freedom using high precision slideways or bearings and equip each resulting axis with single-axis position sensors, such as encoders or interferometers. Alternatively, less constrained kinematic systems often require large reference geometries (e.g. optical interferometer mirrors) built to even tighter tolerances [5]. Nanopositioning stages often use flexures (at the expense of travel range), and usually one-dimensional optical, capacitance or strain gauges sensors are integrated into the stage. These systems and sensors require calibration and error mapping to obtain optimum performance [6]. Optical interferometry has been the preferred route to their characterisation and calibration [7]. However, Abbe errors and thermal distortions, major sources of error in dimensional metrology, ultimately limit the performance of one-dimensional position sensing. Full 6-degree-of-freedom (6DoF) characterisation, sensing and control therefore becomes necessary. Even with extreme mechanical finesse, advanced nanopositioning systems would ideally have 6DoF measurements taken close to the point of interest (sub-millimetre) and thus call for compact (millimetre-size) components.

Diverse multi-axis metrology approaches have been proposed for a more complete and thereby more accurate measurement of position. Some based on optical interferometry [8,9] and others on 2D patterned scales encoder-based systems [10,11,12]. Multidimensional, absolute positioning systems based on a reference pattern, also known as self-location, have long been studied as a discrete mathematics coding problem [13], and as a broader engineering challenge for diverse applications such as camera pose estimation.

While laser interferometry has developed tremendously since inception, over the same period, Moore's law has ushered in ubiquitous computing, high-resolution image sensors, and the photolithography industry. This combination now lends itself to new sensor paradigms. In this work we present a novel 6DoF position sensor technology and validate it to sub-nanometre precision in two dimensions against world-class traceable optical interferometers in a temperature-controlled laboratory.

Anemos MAPS

The Multi-dimensional Absolute Position Sensors [14] comprises three subsystems described in later sections: a reference scale, a camera, and a computer image processor (Figure 1) that determines the position of the camera relative to the scale.

The proprietary 2D scale pattern has a digital signature modulating dot sizes in a regular array. This provides absolute (unique) position information from which locations in six axes are derived simultaneously for each captured video frame or sample. It improves on previous work [10,15] by providing a near-homogeneous, DC-balanced pattern designed to enhance interpolation, and robust 4-quadrant decoding (finding the 2D coordinate of each dot under any rotation/translation). Absolute position is obtained from concatenating decoded digital (linear integer address or rotational quadrant) and interpolation (fractional) parts for each axis.

Of the six axes, yaw, X and Y measurements are practically independent of optical path length and require no additional calibration (the scale establishes the metrological reference). The further three axes depend on optical magnification in deriving Z and roll/pitch by perspective analysis, and cameras need calibration after manufacture. Resolution and accuracy of Z, pitch, and roll are up to two orders of magnitude worse than the planar axes. In these experiments pitch and roll variation (stage motion errors) were too small to be usefully assessed and only results for the other four axes are documented in this paper.

MAPS uses off-the-shelf electronics components, optics, and simple LED illumination within custom-built systems that are tailored to reduce thermal, mechanical, and optical effects. For this work four custom camera versions were built, and processors updated twice.

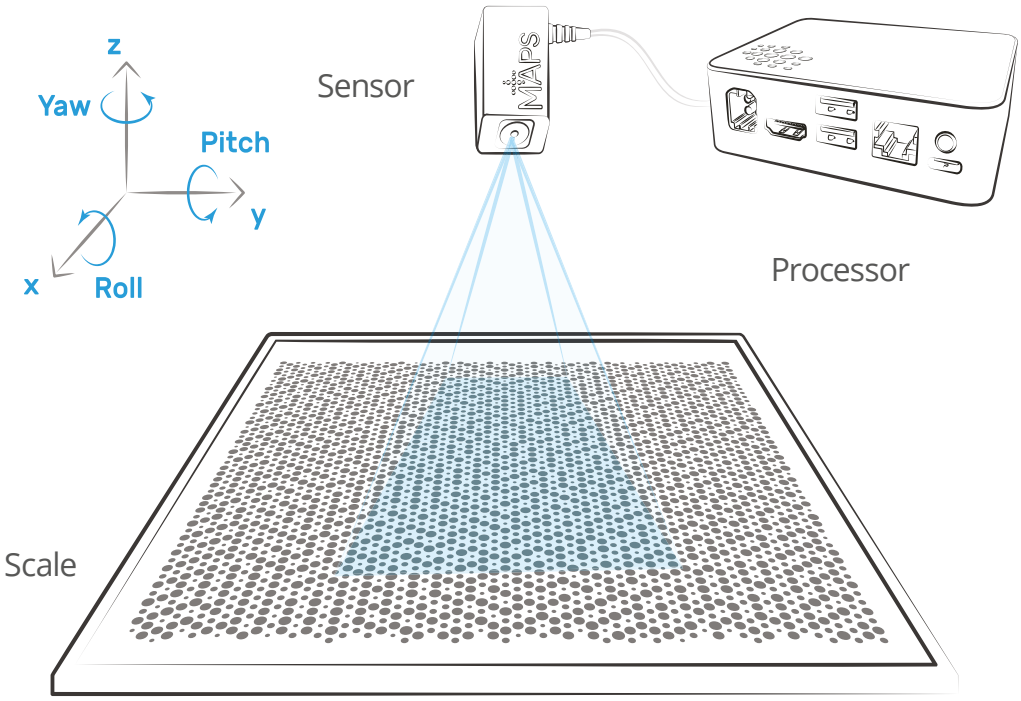

Figure 1. Conceptual system diagram of the Anemos MAPS

General MAPS advantages and disadvantages

In many ways MAPS features contrast with and complement OI capabilities. MAPS principal advantages include absolute 6DoF measurement at the point of interest, near identical operation in vacuum and air, high resolution independent of travel distance, manufacturing variance compensation through error mapping, and very broad cost/performance scalability. Disadvantages include low bandwidth, power dissipation, and increasing scale cost with measurement envelope.

MAPS systems are insensitive to ambient air conditions and require no correction for atmospheric changes. This is because imaging geometry (determined to the first order by the ratio of lens to scale and image sensor distances) is unaffected by the refractive index of surrounding air which instead affects miniscule changes to focus or blur. In principle, dynamic air conditions (large pressure/temperature gradients) could cause prismatic effects that bend (mirage) or distort the image view resulting in error, but this will be insignificant with a short optical pathlength, as used in this work.

Resolution and short-term accuracy are both constant at any travel position within MAPS operating envelope (XY scale size, unlimited yaw, z-pitch-roll values that maintain reasonable image focus/contrast). Again, scale quality and physical stability fundamentally establish absolute dimensional accuracy. This is both a major advantage and burdensome. Mainstream high-accuracy low-cost lithography exist for printing small “chips” to multi-metre-square scales (LCD panel manufacturing) and in many nanoscale applications, the diminutive scales represent a small fraction of overall system cost (far cheaper than OI mirrors). However, in large-travel applications, mechanically and thermally stable scales and their support structure may become prohibitively expensive as costs climb with surface area.

Another key benefit of MAPS is that its resolution is not limited by analogue to digital converter bit depth (such as those in OIs). Position calculations convert a hundred million bits of information into 53-bit mantissa results and in this sense “resolution” is theoretically unlimited. Meaningful and useful resolution is limited by intrinsic noise, and this has been the subject of intensive investigation both through experimental techniques presented here and extensive simulation. Experiment and simulation indicate that the MAPS noise floor for XY measurement should be in the picometre range or 40-bit resolution over metres of travel.

A detractor for MAPS is its low bandwidth which is limited to video capture rates (60 Hz in current Anemos designs, although cameras with kilohertz acquisition rates are available today). Processing power constraints are less of an issue for previously stated reasons, low bandwidth, and through algorithmic optimisation. While MAPS sample rate is relatively low, temporal acuity on the other hand can be exceptionally high. Strobed illumination can capture motion with microsecond resolution, and synchronised sampling of repetitive motion can be used to synthesise higher bandwidths than generally possible by other continuous methods.

Another potential problem is self-heating. In these experiments, MAPS cameras each dissipated approximately 100 mW within a few centimetres of the work point (orders of magnitude higher than laser mirror heating), but various mitigation techniques are applicable such as active temperature control of the camera system.

Last is scalability. In addition to evolving with cost reductions, integration and miniaturisation advances in the electronics industry, MAPS price-performance is configurable for diverse applications. Camera resolution and scale quality determine resolution and accuracy. The speed of the system is determined by the maximum camera frame rate and the computing power available to decode images in real-time. For example, a basic system could use mobile phone camera and app using scales printed on paper whilst the more advanced system used in this work requires photolithographically defined scales to achieve better performance.

Scale

The scales used in this study were printed chrome on quartz glass using mask-making equipment and patterned with the MAPS scale pattern at 5 µm grid pitch. The relatively low-end (critical dimension greater than 2 µm, 500 k dots per inch) mask writer used in initial scale production introduced a noticeable modulation pattern in the X direction. These micrometre-level inaccuracies were nonetheless successfully decoded to yield nanometre XY and µradian yaw precision, though compromising other axes. In subsequent tests this was corrected using a more advanced photolithography tool. As the metrological reference, scale defects directly affect accuracy. Short term variations (small dot offsets, local glass roughness, dust, and detritus) tend to be aggregated and averaged away, and longer-term variance (lithography errors, scale bow, rotation and offset) can be “mapped” and compensated for after installation.

Camera

Two cameras were used in these tests: firstly 1 Mpixel, then 9 Mpixel in the upgraded version. Both had image sensor PCBs glued to large aluminium blocks for high mechanical and thermal stability. The lens common to all setups was a low distortion x4 microscope objective with a field of view around a square millimetre on the scale. The lens was mounted separate to the image sensors and in solid aluminium mounts. Note the camera image sensor’s susceptibility to thermal effects or vibration is reduced by the optical magnification factor, all other things being equal.

Processor

Processing each sample image uses billions of operations to yield 64-bit floating point results using proprietary algorithms developed at Anemos that leverage the benefits of the scale pattern. Over the course of these experiments the image processor evolved from a PC through two generations of embedded GPU systems and software also advanced over several code generations. .

Predicted accuracy and resolution

Noise figure assessments, MAPS to MAPS correlation, and simulation, provide a broader picture of MAPS (and OI) potential. For instance, Z and yaw accuracy and noise are useful proxies for XY performance, as described later. As mentioned above the theoretical resolution of the system is limited by actual noise, which is defined as a 1-sigma measurement variance or error.

Expectations of resolution and accuracy performance are set by extensive simulation used by Anemos in quality assurance and design optimisation. System modelling has extremely fine control over 6DoF motion and many other variables (camera noise, blur, lens distortion, and so on) in generating synthetic images which are then decoded and assessed for error. Figure 2 illustrates an idealised (no noise) synthetic image alongside a real, but poor-quality camera capture. This modelling provides much faster and wider test coverage than possible in the physical world. Based on simulations and given the limited motion (pitch and roll in particular), the experimental setups could be expected to achieve better than 100 pm accuracy and picometre noise levels.

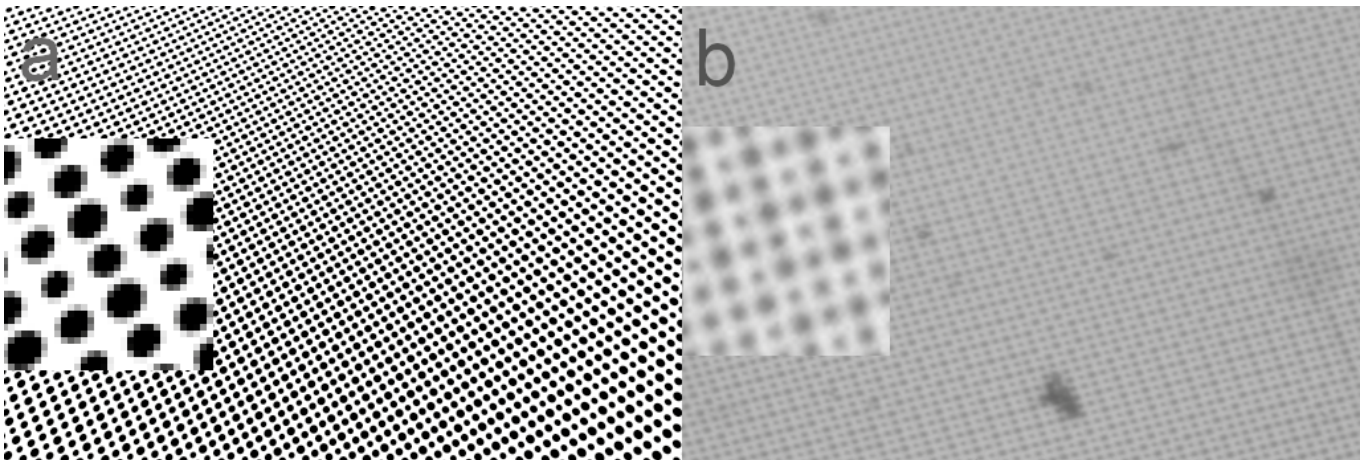

Figure 2. (a) Synthetic test image generated with exaggerated lens distortion and perspective, but no noise or blur. Zoomed pixel-perfect patch inset. (b) Cropped section of a low-quality (but still viable for reliable decoding) real image with noise, blur, detritus, poor contrast, and zoomed patch inset.

Experimental configuration

Results presented in this paper come from three experimental setups. Two at NPL which used optical interferometers to provide a traceable reference measurement to probe accuracy and resolution, and a third at Anemos for analysing system performance, principally resolution and noise, including statistical treatment of large datasets.

The interferometers used are homodyne Plane Mirror Differential Optical Interferometers produced in-house at NPL [16]. Amongst other advantages, a differential configuration reduces measurement loop, dead path, and sensitivity to environmental fluctuations. Interferometer outputs are conditioned by bespoke transimpedance amplifiers and then converted using an FPGA system that applies a Heydemann correction to remove non-linearities [17]. Additionally, the air temperature, pressure and humidity were recorded for subsequent Edlen corrections to account for changes in refractive index of the air [18,19].

Setup one

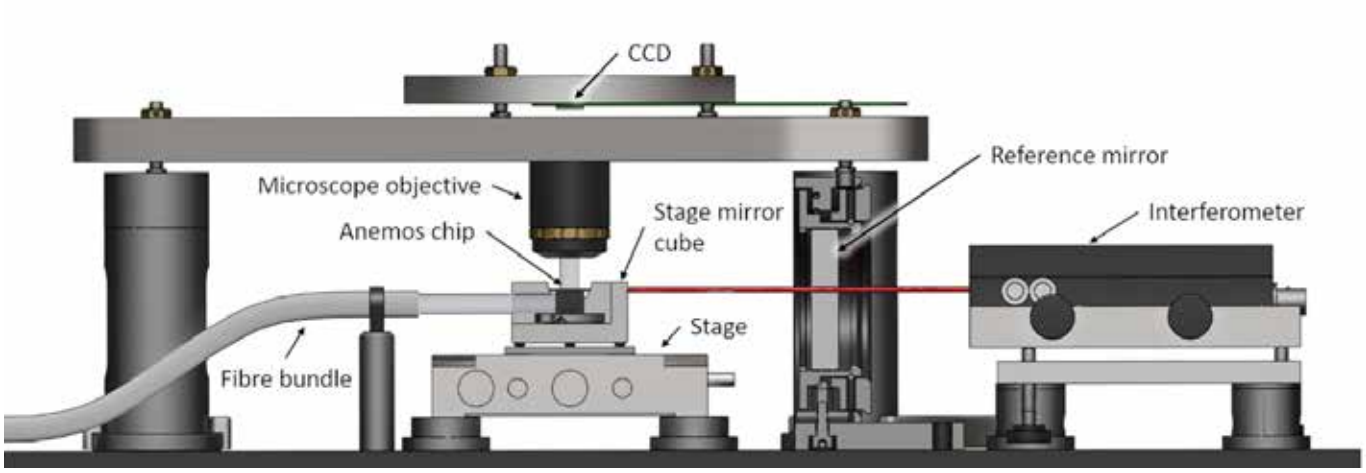

Figure 3. A side view of the experimental setup showing the key components. The Y axis interferometer components have been omitted for clarity. The X axis reference mirror mount is shown in cross section to show the mirror position within.

The first experimental setup for comparing MAPS with interferometry was constructed at NPL. This was based on the existing NPL stage test rig [6]. The rig comprises three interferometers pointing at three orthogonal sides of a precision mirror cube mounted on a stage and two autocollimators to measure angular errors in the stage motion. This allows the motion of a translation stage to be mapped, usually comparing the positions measured by the interferometer to those reported by the stage's internal sensors. The interferometers provide traceability to the SI metre via the use of stabilised HeNe lasers calibrated against NPL's primary metre realisation laser [20].

For the purposes of this work the z-axis interferometer was discarded and the mirror cube replaced with a cut-out cube that that allowed the MAPS scale to be mounted between the mirror faces (Figure 3) facilitating comparison of interferometer and MAPS measurements as the stage is moved. The translation stage (Queensgate NPS XY 100) used for this setup was servo controlled and had a scanning range of 100 µm in the X and Y axes.

Placing the MAPS scale within the mirror, at approximately the same height as the interferometer beams, reduces the Abbe error of the system. The MAPS camera is placed above whilst illumination comes from the side, transferred through the scale via a beam splitter below the scale.

Tests were carried out by driving the stage along a scan path and taking measurement from the OI, MAPS and the stage sensor at each point on the path. The scan paths were generated using the Gwyscan path generation library [21]. Due to the substantial differences in measurement systems, achieving perfect synchronization between them was not possible and a "move, wait, measure" strategy was employed. This measurement strategy relies on the stage remaining still during measurement and previous experience with stages of the same type used in similar experimental setups suggests that this is the case within a tolerance of a few nanometres.

Setup two

Later experiments carried out at NPL used one OI and four MAPS sensors/scales attached to a higher precision single-axis translation stage (Queensgate NPS-X-28C). The MAPS scales were mounted on a cube such that each of the MAPS systems was independently measuring the same motion along the stage axis. The mirror for the interferometer was also mounted on the cube to give a reference measurement along the stage axis. This setup was designed to give a far richer dataset from which to analyse system kinematics. The same interferometer design was used as in the previous setup. The scales were illuminated from behind using LEDs embedded into the mounting cube.

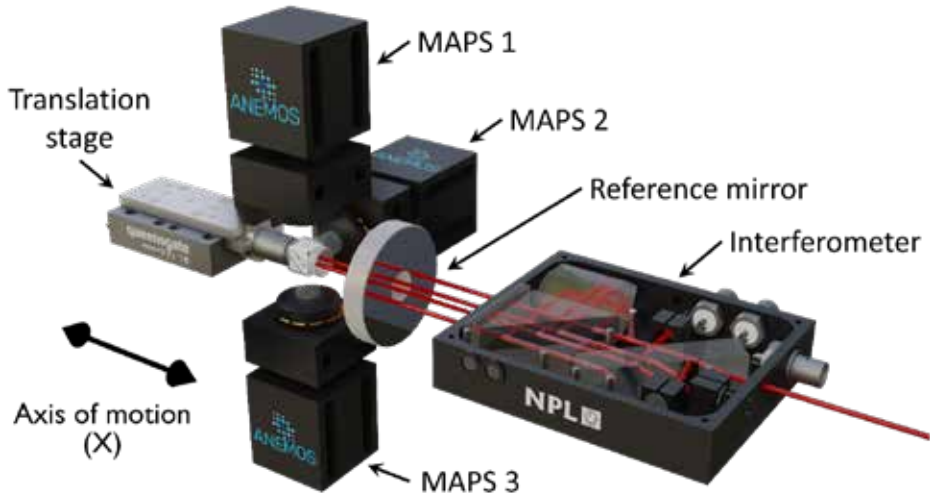

Figure 4. Experiment's CAD model with OI system in the foreground, MAPS cameras behind, and stage at rear. The camera for MAPS 4 and mounting hardware has been omitted for clarity. Note that the X axis is common to all measurement systems and is along the axis of motion. The Y and Z axes of the MAPS systems are defined individually for each system such that Z is the direction perpendicular to the scale plane, and Y parallel to the scale and perpendicular to X.

Setup three

Following completion of work at NPL, supplementary measurements were undertaken using a single MAPS (experiment 2 version) and an XYZ nano-stage system made in-house at Anemos [22]. The stage's travel range of just 10 nm and open loop control allow D/A noise and servo effects to be completely discounted. MAPS was also configured for faster sampling and less averaging since synchronisation was obviated. Large drift (>100 nm) due to the uncontrolled thermal environment and absence of closed-loop control made the system much less stable than similar MAPS configurations operated at NPL. However, the installation collects mega-samples over weeks of continuous operation.

Data collection and processing

Data was collected using two separate programmes communicating over a local network. One controlled the stage motion and collected the interferometer data using an FPGA interface to carry out fringe counting. The other ran on the MAPS system which collected images and processed them to decode position.

The stage controller programme sent messages to the MAPS system signalling to it when to collect data. Data was saved in separate log files (including environmental parameters for Edlen correction) for each programme with identifier numbers so the databases could be later reconciled.

The data processing followed the following steps. First, the two datasets were combined using the identifier numbers to align them. Next the two data sets were aligned in space by first subtracting the values of the first coordinate from each data set (X interferometer, Y interferometer, X Anemos, Y Anemos) so that the first point of the scan was set to (0,0) for all position sensors. Following this (for multiple axis data) the data was manipulated to align the axes of the two data sets. This rotation is required because the axes of the MAPS measurements were not perfectly aligned with the those of the interferometers. It also allows the use of MAPS scales at arbitrary angles. Four methods were used for this rotational alignment:

0. None.
1. Rotation of the MAPS data by an angle θ about the new origin such that the sum of the squared differences between the MAPS and interferometer positions were minimised.
2. Perspective fitting to compensate for relative tilt between the scale and plane of stage motion.
3. For the data presented in Figure 9c/d/e estimated stage drift was removed to better compare detail with moderate high-pass filtering. Specifically, a 5th degree polynomial was fitted to the data and then subtracted to remove slow changes in motion.

After the axes are aligned it is possible to calculate the differences between the interferometer and MAPS data sets. Differences were calculated individually for each axis and an additional combined scalar difference (for 2D data) was calculated by adding the X and Y differences in quadrature.

Results

Setup one results

A series of scans were made following different paths. On all these scans it was noted that the agreement between the Anemos system and the interferometers for the x-axis data was not as good as that for the y-axis data. This disagreement in the x-axis data appeared consistently across scans made with the scale and camera rotated relative to one another and consistently across scans made with different paths. An example of these 2-dimensional scans is shown in Figure 5.

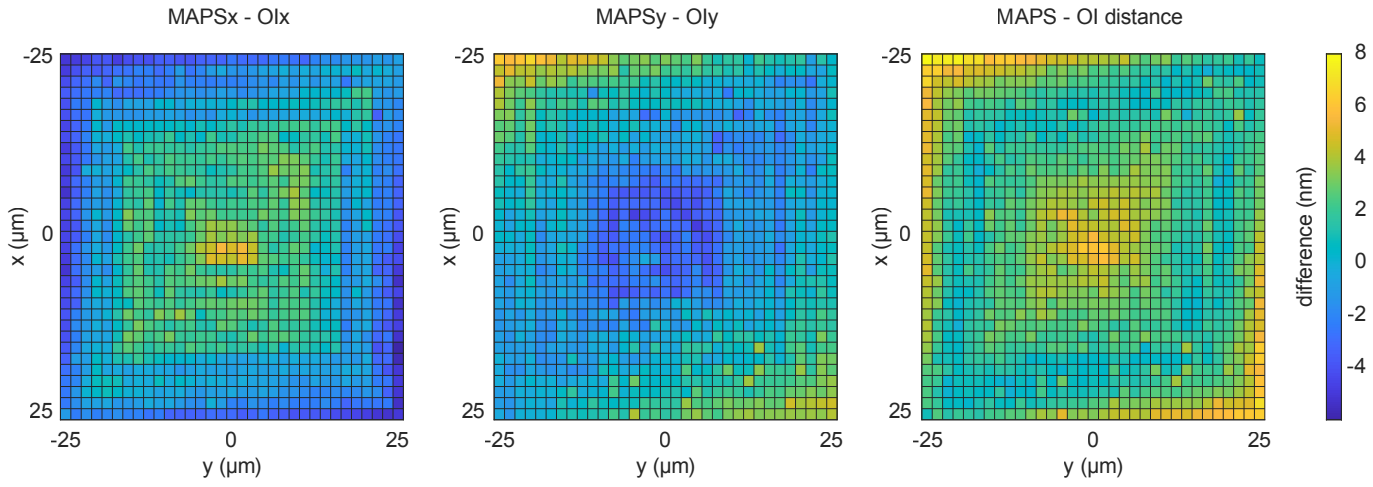

Figure 5. Differences in MAPS to OI measurements traversing a spiral path

The consistency between measurements using different paths even after rotating the MAPS scale suggests some external factor is responsible for the X-axis disagreement. For example, one possible explanation is a change in tilt as the stage moves along the X-axis. It was concluded that scans using only the Y axis could be used to examine the system behaviour in more detail and still be representative of the general 2D accuracy of MAPS.

This system repeatability for arbitrary yaw angles was verified by rotating scales 90° and separately the camera by 120°. These three reconfigurations highlighted no appreciable measurement difference. Of possible sampling regimes, slow, multi-frame averaging was chosen for MAPS sampling. This had an equivalent effect to a 10 second exposure with the intent to smooth out some vibration and noise. This had an equivalent effect to a 10 second exposure with the intent to smooth out some vibration and noise.

Data from a linear scan is presented in Figure 6. The scan followed a line, of length 20 µm, in the Y direction and then returned to the starting point along the same line. For this 1000-sample scan, differences between the interferometers and MAPS were less than 10 nm.

Figure 6 shows that errors are within 5 nm, but probably exacerbated around change in direction of each driven axis. Looking at a detail of the MAPS data near the turnaround, it can be seen that noise and repeatability is at the sub-nanometre level. This suggests that the larger discrepancy seen at the beginning/end of the data (away from the turnaround region) is due to a low frequency drift in the measurement system. As such, it can be concluded that, whilst the accuracy of the system is a few nm the resolution is significantly better.

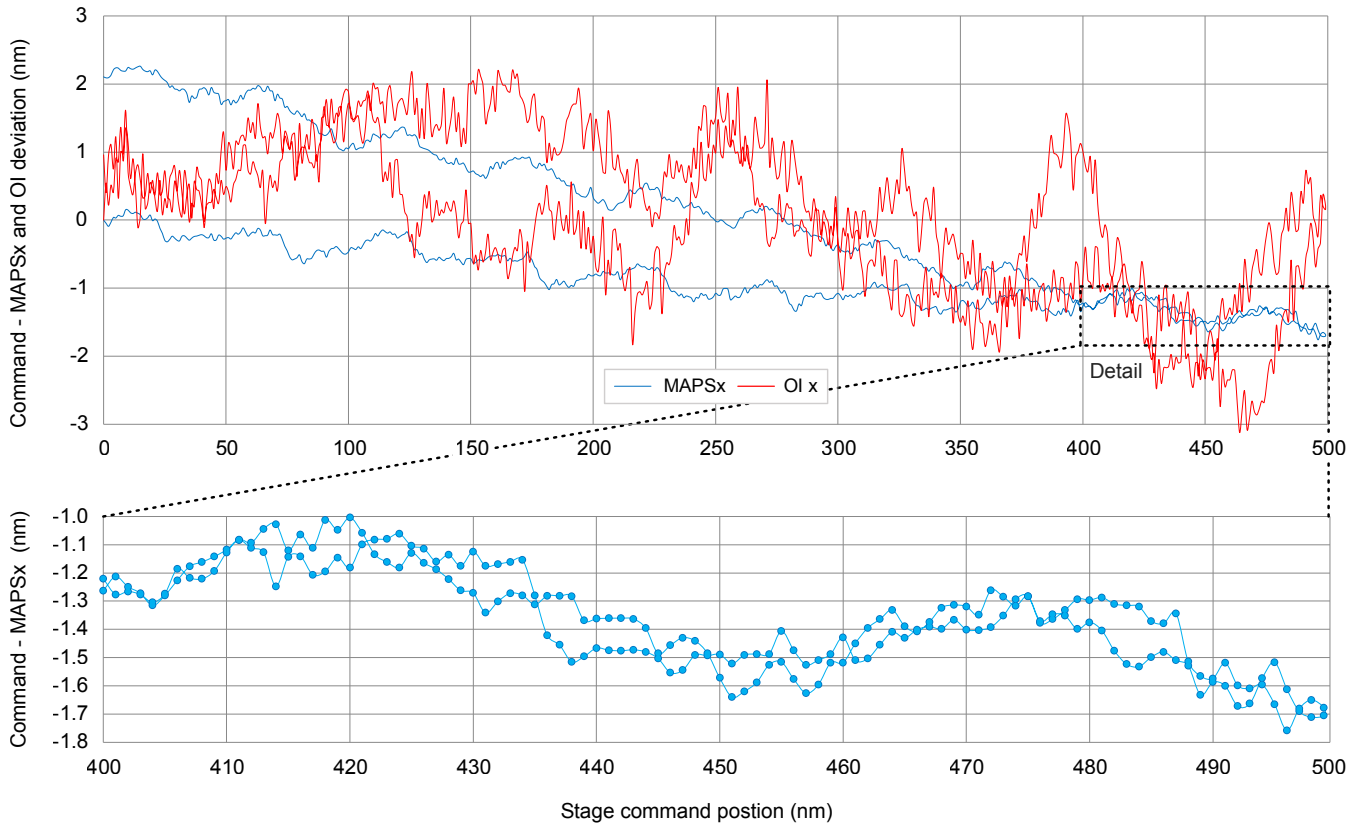

Figure 6. Deviation from command position 500 nm bidirectional linear move (nm) Detail from previous graph illustrates MAPS' resolution and repeatability in the absence of low frequency drifts.

Setup two results

The second setup yielded substantially improved results with nanometre-level agreement between sensors, though Abbe errors and an unidentified source of drift were apparent. Again, this was as much an examination of off-axis motion as absolute accuracy. The limited dataset, small travel, drift and noise precluded rigorous 6DoF calibration of the sensors against each other (26 measured axes, 1000 points). However, sets of MAPS axes do show remarkably coordinated patterns, Figure 8d for example. This provides insight, if not quantification, into the complex off-axis motion path. Perfect X-axes motion would reveal no information in other dimensions, but off-axis components with a dominant motion, to the first order, shared by disparate axes of the four MAPS

does provide a testing ground for MAPS. The dataset indeed includes these artifacts and the cross-correlation of Y and Z, X and yaw are described below.

In Figure 7a, four X axis results are correlated to the OI showing multi-nanometre errors and substantial drift. MAPS_1x deviates noticeably further than other sensors, presumably because its frame of reference was offset from other MAPS and more susceptible to the unwanted stage rotations (the experiment was hand assembled without attempting micron-level component alignment). When the four MAPS result are averaged, however, the results very closely follow the stage command position and stage position sensor, Figure 7b. Opposed sensor pairs effectively null pitch and roll errors around the centre of the cube since their Abbe terms are opposite in sign. Furthermore, comparing residual errors of MAPS and OI (their distance from command position), Figure 7c, strongly correlated patterns suggest both suffer predominantly from the same out-of-plane motion and stage sensor feedback error rather than their intrinsic inaccuracy limitations.

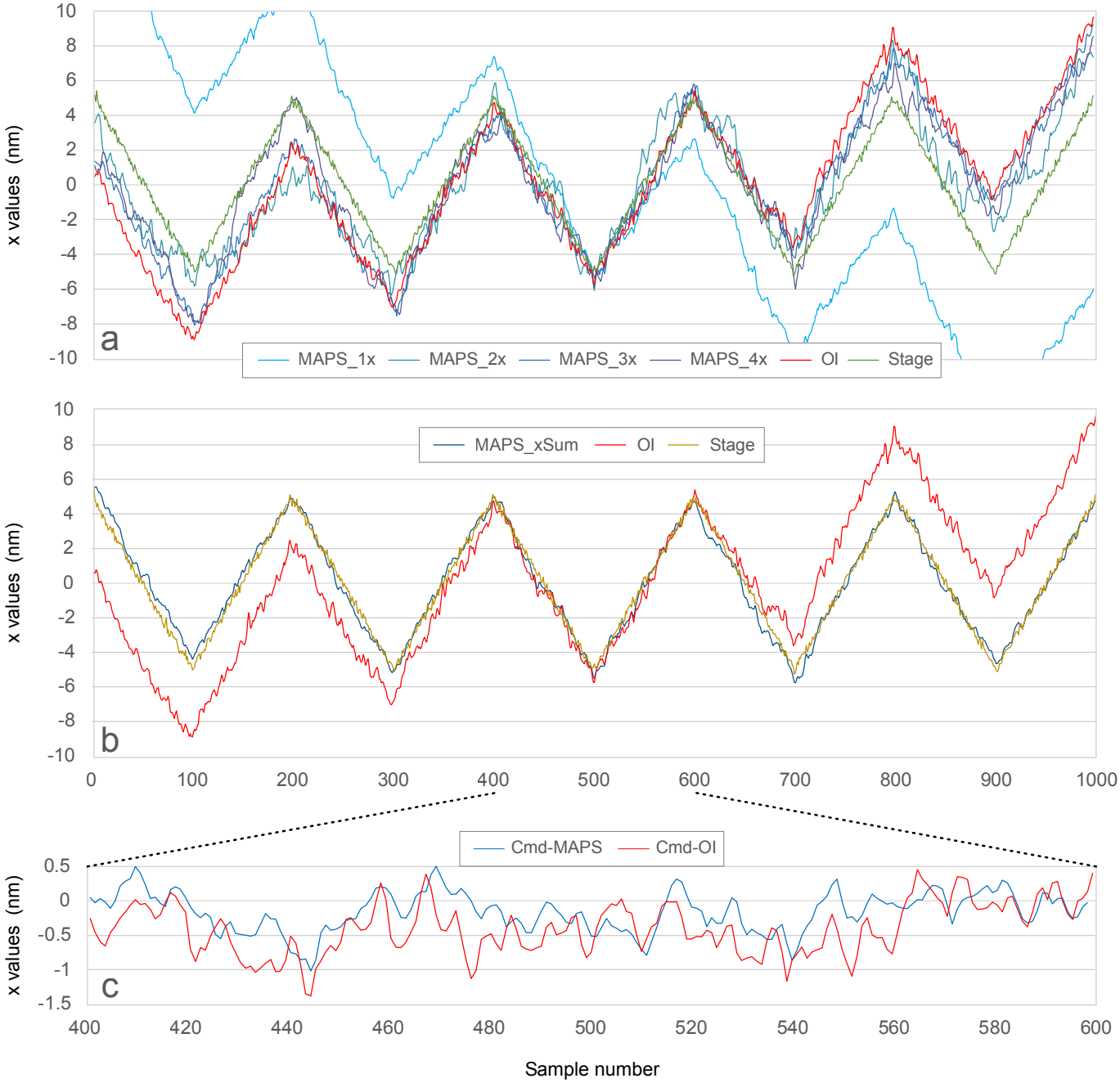

Figure 7. (a) Four MAPS and OI X axis (raw data). (b) Four MAPS_x average, stage command position and OI. (c) Correlation between MAPS_x average and OI difference from command position, central motion cycle.

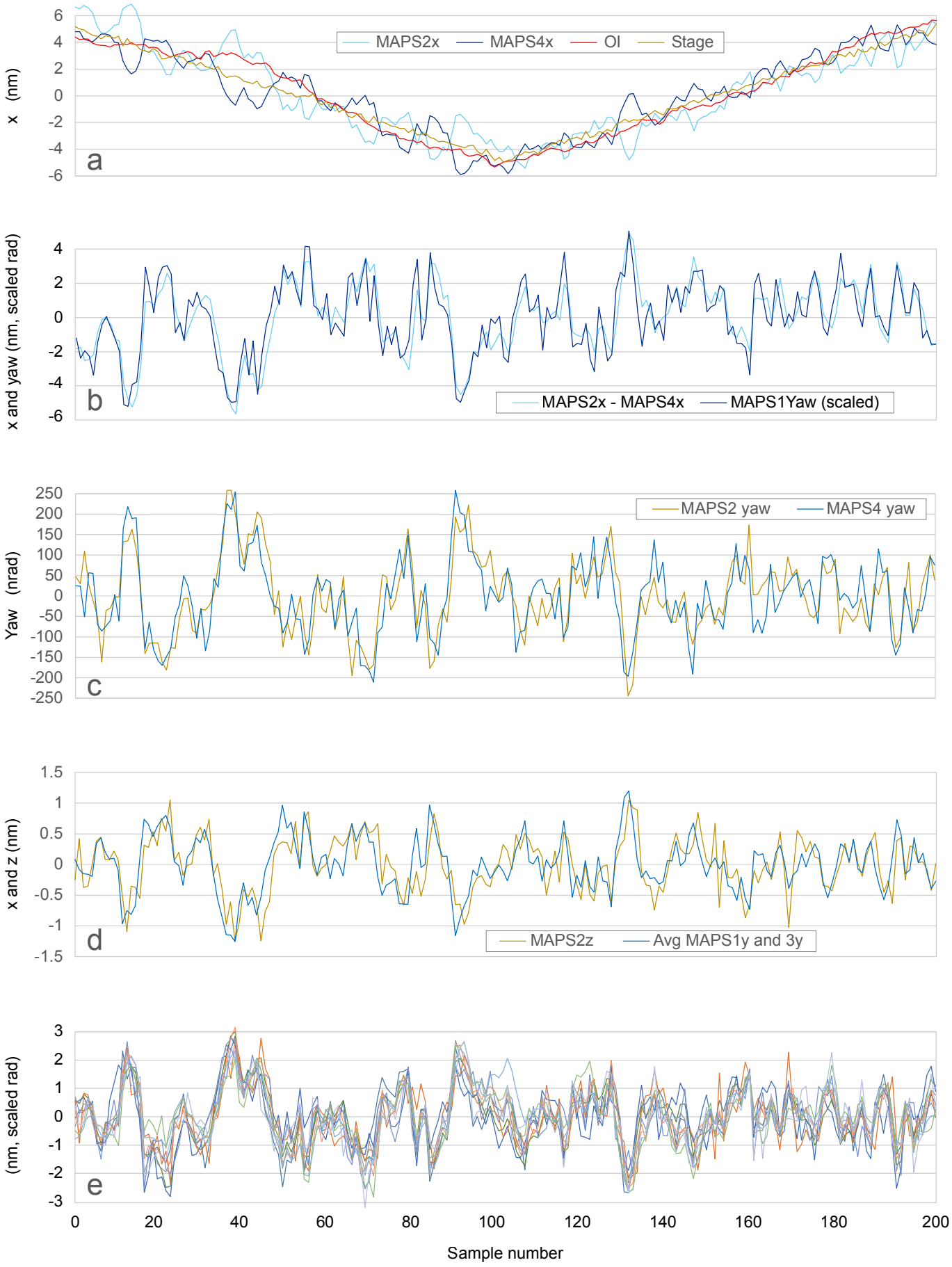

Figure 8. (a) Stage, MAPS 2x-4x, OI data, detail from one motion cycle. Note antiphase peaks in MAPS 2x-4x that correspond to MAPS1 yaw. (b) MAPS2x and MAPS4x difference to scaled MAPS1 yaw (1.4 µrad pk-pk). (c) Fitted rotation on opposite sides of the cube, MAPS 2 and 4 Yaw. (d) Average of MAPS1y and MAPS3y, and corresponding fitted Maps2Z

The difference of two X translations separated at a distance (scales on opposite sides of the cube) correlate well with MAPS2yaw, Figure 8b. The 1.4 µrad amplitude with 10 nm X-differential is consistent with the roughly 14 mm combined cube and scale dimension. Plotting two other opposing sensors' yaw values, Figure 8c, also shows a match generally to within 50 nrad of each other, but with 150 nm outliers.

Likewise, averaged Y displacements on two opposing sensors corresponds to Z displacement on orthogonal sensors. Figure 8d demonstrates this correspondence within approximately 500 pm with discrepancies also clearly correlated to other axes' artifacts. This result is of particular interest since Z is a "weak" axis of MAPS compared to XY.

Open loop nanopositioning results

While moving the stage in approximately 1 nm circles, 250 000 data points were measured for analysis. The circular motion superimposed on large drift, Figure 10, was a real time plot grabbed during accelerated temperature change. FFT spectral analysis, Figure 9, shows classic 1/f noise shaping, and the FFT plot of yaw illustrates a sub-µrad parasitic, out-of-plane, angular motion.

When frequencies below the deliberate stage excitation (presumed to be related to thermal drift) are removed with a high-pass filter and the full XY data replotted, Figure 10, a system noise spread of 25-35 pm can be approximated from the chart. The angled, elliptical motion was due to a variation in XY stage gain with the scale set at an angle to the camera. Noise variance with angle may be due, for instance, to axis-related stage stiffness and vibration sensitivity.

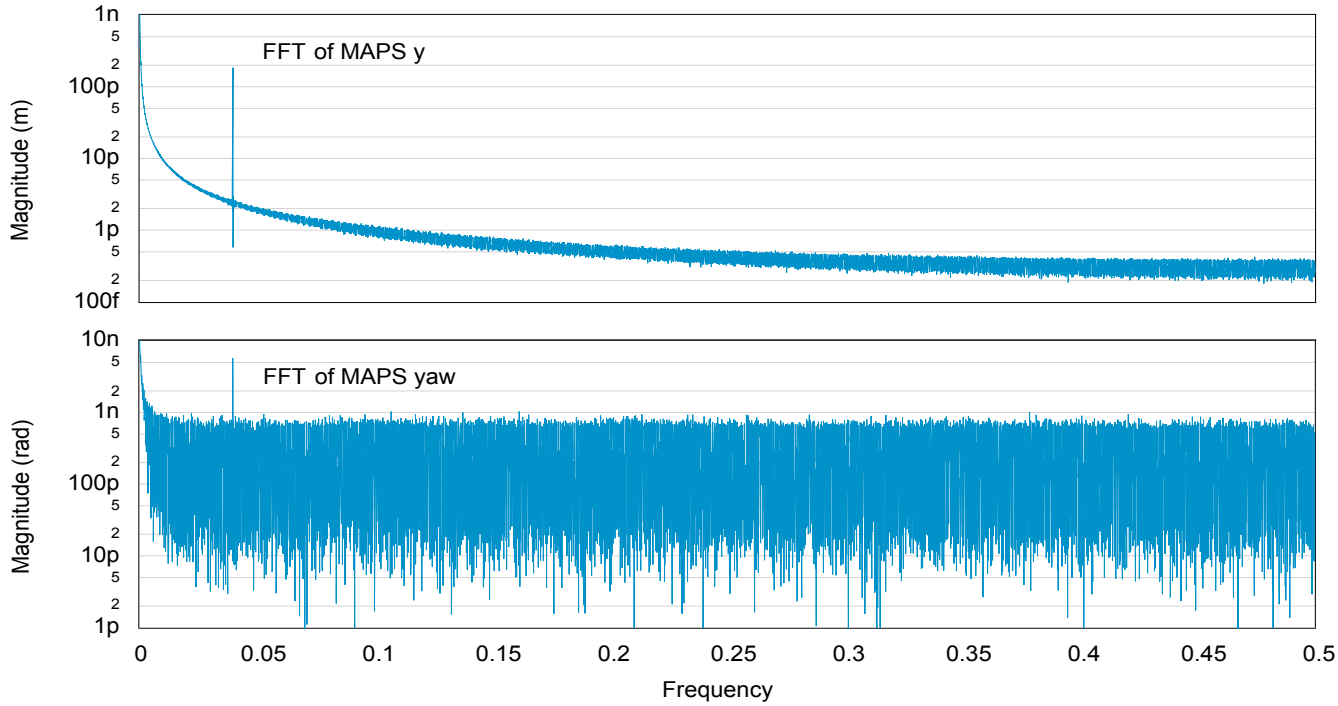

Figure 9. FFT plot of 250k X and yaw samples for 1 nm circular motion (zero-frequency spikes are cropped).

Filtered XY samples expressed in polar coordinates were used to better quantify 1-sigma system noise by three methods: the standard deviation (root sum of square difference from mean) over all radii from a fitted ellipse; standard deviation of radii over each of one thousand bins sorted by angle; and counting 86 % population spread for each bin. The results were 50 pm, best case bin 35 pm, best bin 25 pm, respectively. Note, noise figures still include residual thermal noise (piezo, lens and camera were not temperature immune), and vibration noise (higher frequencies). Certainly, large step perturbations were observed (in an otherwise unusually quiet location) which correlated with personnel movements in the lab and extreme weather events. In fairness, low frequency noise belongs, in part, to MAPS and gives only an indication of potential rather than actual performance. Certainly, better experimental conditions and broader use of low-thermal coefficient of expansion materials in construction would improve these findings.

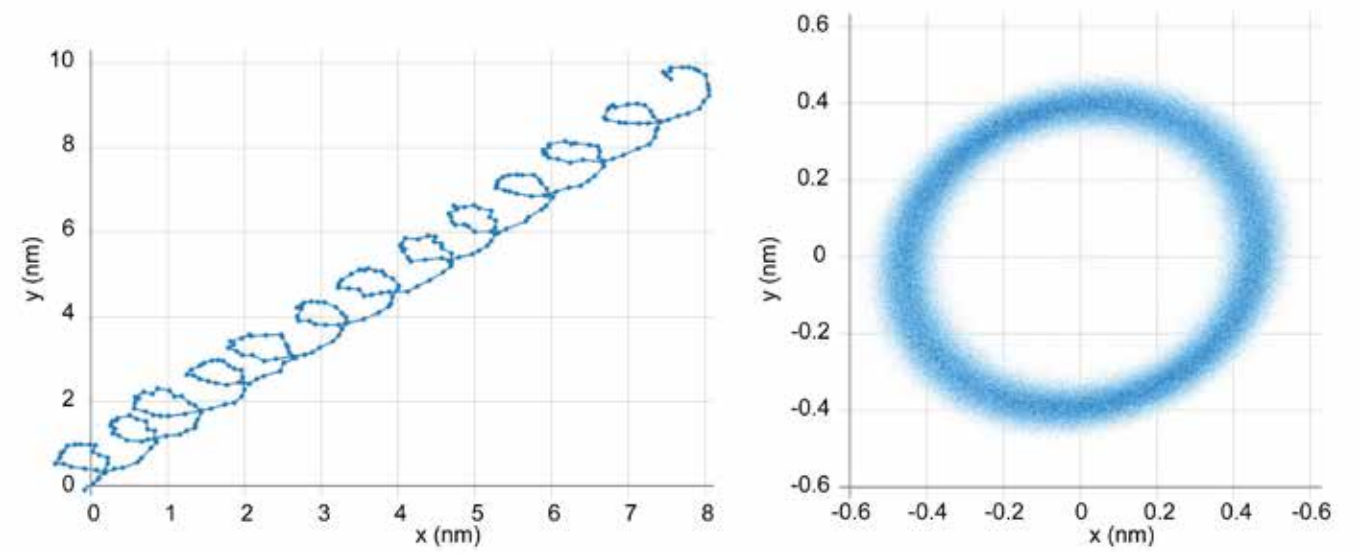

Figure 10. Sample XY trochoids formed from 1 nm circular motion with system drift (dots are sample points), left, and scatter plot of 1 million hi-pass filtered XY MAPS readings, right.

Discussion

Attributing nano-scale dimensional observations and artifacts to specific error mechanisms, remains challenging. However, extreme-resolution multi-axis and multi-sensor configurations provide insight into some behaviours impossible to "see" using any single axis sensor, for example the curious sub-nanometre sawtooth response in Figure 6.

Yaw and Z noise serve as proxies for translation, XY, resolution since both are derived by essentially linear measurement. Usefully, mechanical yaw noise in these experiments is more contained relative to XY variations.

With the scale image field of view of 1 mm, yaw is calculated from linear XY differentials across quadrants with a 0.25 mm median radius. Therefore, the measured yaw noise of approximately 20 nrad corresponds to resolving 5 pm linear scale movements. This system level measurement still includes actual mechanical yaw on top of inherent MAPS errors. Nonetheless, it indicates actual MAPS performance approaches modelled precision (better than a million-to-one grid interpolation). Sample to sample noise estimates (deviation from a straight line) from early experiments also corroborate angular system noise at around 20 nrad, as does the FFT analysis. MAPS determines Z from the image by assessing XY pitch or image zoom. Given the setup's optical geometry, Z requires approximately 50 times better system performance than do X and Y. In other words, Z following Y within 500 pm, implies an XY resolution level also below 10 pm.

Measurement artifacts seen are unlikely to be MAPS related. The four channels of the last experiments were completely independent, each with subtly different setup angles and relatively large XYZ offsets, and no intrinsic mechanism exists for the fine inter-channel or inter-axis correlations observed. The medley of measurements in Figure 8d can only relate to real motion.

The heavy use of image averaging to mitigate stage noise and synchronization challenges, and its concomitant signal bit-gain from 10-bit greyscale to 18 bits, draws into question the extent to which reducing MAPS camera noise improves accuracy. To evaluate this, a set of six thousand real images were decoded at various bit-depths (truncated to fewer binary digits), and discrepancies to original results graphed (Figure 11). Impact of averaging was indeed minimal (a few pm) and MAPS XY noise was low compared to other sources – even if no averaging had been employed or image quality diminished to as low as 6 bits/pixel. However, noise reduction would benefit more the angular and Z measurements. The corollary to this analysis (also supported by simulation) is that for images with noise below the eighth bit, camera noise results with less than 10 pm XY noise. Finally, the scalability of MAPS means enhanced image sensor resolution, finer scale pitch, better image contrast, for example, can collectively improve measurement accuracy and resolution by an order of magnitude.

Although an uncertainty budget was not produced for the experimental configurations here, based on similar work [6], the expected uncertainty for the interferometer measurements is likely to be < 5 nm across the full range of the various stages used, the most dominant components of which are likely to be associated with refractive

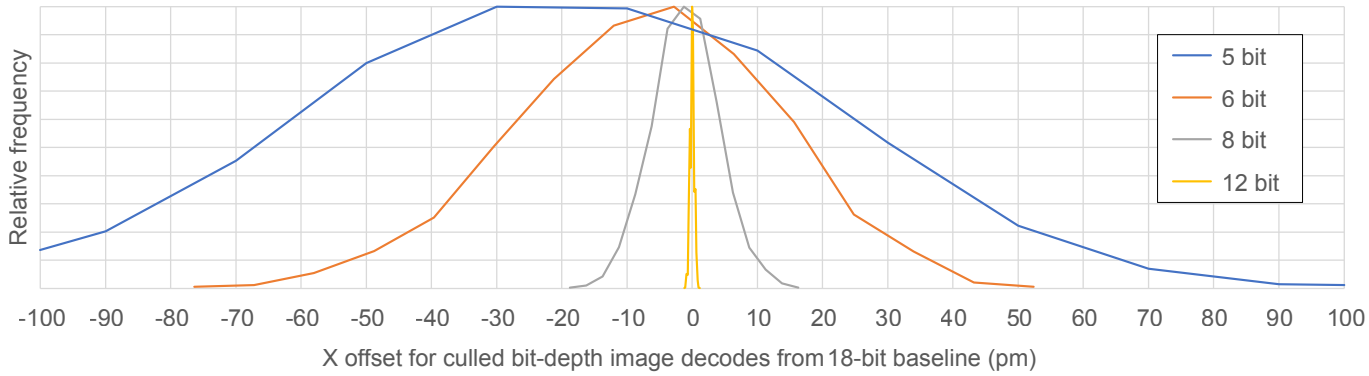

Figure 11. Histogram of X decode error estimation with fewer bits per pixel.

index uncertainty on the interferometer dead path correction and potential Abbe error. This is consistent with the experimental observations reported here. Overall accuracy of MAPS will ultimately be dependent on the fidelity of the grating and its calibration. During the lifetime of the experiments, there was an improvement in the quality of gratings produced and used.

For the MAPS system, errors are likely to be in the printing of the scales, pitch error and any non-linearity in the scale over a longer range.

Conclusion

A series of experiments using state of the art, traceable optical interferometers at NPL validated MAPS XYZ axes accuracy to be within 5 nm and precision to better than 1 nm after accounting for off-axis nano-stage motion. Abbe errors were an apparent limiting factor in test results, but single-digit-picometre resolution in XY of the MAPS system was also evidenced by direct and indirect measurement. The resolution of the MAPS system is further confirmed by independent MAPS systems all measuring the same motion and agreeing to within a few tens of picometres and tens of nanoradians.

MAPS 6DoF characterisation provided insights into real-world behaviours of nano-positioning systems. These novel capabilities of MAPS´ coupled small size and scalable performance, bode well as a potential reference artefact not just for nano-scale metrology, but also in larger range CMM/CNC calibration, microscopy, AFM, robotics, and many other applications.

Future work

This work investigated small movements and tiny off-angle errors that are beyond current pitch/roll measurement capabilities. Future work over longer travel distances and more detailed characterisation of all axes is planned with 6DoF positioning stages and multiple OIs operating in a vacuum rather than air.

It is also proposed to investigate how the MAPS scales and camera systems can be calibrated in a suitable way to provide traceability to all axes of MAPS measurements.

Acknowledgements

We thank Innovate UK for funding from the Analysis for Innovators (A4I) Programme.

Rob Ferguson (NPL) is thanked for help with component assembly and NPL Engineering Services are thanked for mechanical components manufacture. Alison Raby from Queensgate Instruments, a division of Prior Scientific, is thanked for loan of a Queensgate XY and linear translation stages.
Thanks also the wider team at Anemos for invaluable contributions.

Author contribution statement

Richard Aras designed and developed MAPS and carried out experimental work. James Dallas provided project management at Anemos. Edward Heaps carried out experimental work. László Varga was responsible for software development, data processing and visualisation. Andrew Yacoot provided metrology expertise for experiment design and data analysis. All authors collectively discussed and analysed results and contributed to this manuscript.

Disclaimer

The naming of any manufacturer or supplier by NPL or Anemos in this journal shall not be taken to be either NPL's or Anemos' endorsement of specific samples of products of the said manufacturer, nor recommendation of the said supplier. Furthermore, NPL and Anemos cannot be held responsible for the use of, or inability to use, any products mentioned herein.

ANEMOS Technology Ltd.

100 Fenchurch Street, 4th Floor, London, EC3M 5JD, UK

www.anemos.co.uk, info@anemos.co.uk

The National Physical Laboratory

Hampton Road, Teddington, TW11 0LW, UK

www.npl.co.uk

References

1. Schmitt et al 2016 Advances in Large-Scale Metrology – Review and future trends CIRP Annals 65 643-665 https://doi.org/10.1016/j.cirp.2016.05.002
2. Estler et al 2002 Large-Scale Metrology – An Update CIRP Annals 51 (2) 587-609 https://doi.org/10.1016/S0007-8506(07)61702-8
3. Slocum A H 1992 Precision machine design ISBN:100136909183
4. Dotson C 2006 Fundamentals of Dimensional Metrology ISBN:9781418020620
5. McCarthy K J and Hunter B L, A high performance x-y stage with a novel topology: ASPE "Control of Precision Systems" April 13, 2010
6. Yacoot et al 2019 Design and performance of a test rig for evaluation of nanopositioning stages Meas. Sci. Technol. 30 035002 (10pp) https://doi.org/10.1088/1361-6501/aafd03
7. BIPM, The International System of Units (SI Brochure) [9th edition, 2019], Appendix 2: Practical realizations of the definitions of some important units - Mises en pratique, Mise en pratique for the definition of the metre in the SI, https://www.bipm.org/utils/en/pdf/si-mep/SI-App2-metre.pdf
8. Burt et al 2012 Aperiodic interferometer for six degrees of freedom position measurement Optics Letts. 37 7 1247-1249 https://doi.org/10.1364/OL.37.001247
9. Molnar et al 2016 Simultaneous multiple degrees of freedom (DoF) measurement system Meas. Sci Technol. 27 8 084011 https://doi.org/10.1088/0957-0233/27/8/084011
10. Archer O and Nguyen T-H 2019 Turning a machine vision camera into a high precision position and angle encoder: nanoGPS-OxyO Proc. SPIE 11056, Optical Measurement Systems for Industrial Inspection XI; 110562O (2019) https://doi.org/10.1117/12.2524938
11. Pisani et al 2020 Characterization of Angle Accuracy and Precision of 3-Degree-of-Freedom Absolute Encoder Based on NanoGPS OxyO Technology Sensors 20(12) 3462 https://doi.org/10.3390/s20123462
12. André A N et al 2020 Sensing One Nanometer over Ten Centimeters: A Micro-Encoded Target for Visual In-Plane Position Measurement, IEEE/ASME Transactions on Mechatronics PP(99):1-1 https://doi.org/10.1109/TMECH.2020.2965211
13. Bruijn, de, N. G. (1946). A combinatorial problem. Proceedings of the Section of Sciences of the Koninklijke Nederlandse Akademie van Wetenschappen te Amsterdam, 49(7), 758-764.
14. Aras R, Multi-axis Position Sensing System, UK patent GB2576164.
15. André A N et al 2021 Robust Phase-Based Decoding for Absolute (X, Y, Θ) Positioning by Vision, IEEE Transactions on Instrumentation and Measurement, vol. 70, pp. 1-12, Art no. 5001612, https://doi.org/10.1109/TIM.2020.3009353
16. Yacoot A and Downs M J 2000 The use of x-ray interferometry to investigate the linearity of the NPL Differential Plane Mirror Optical Interferometer Meas. Sci. Technol. 11 1126-1130 https://doi.org/10.1088/0957-0233/11/8/305
17. Peter L. M. Heydemann, Determination and correction of quadrature fringe measurement errors in interferometers, Appl. Opt. 20, 3382-3384 (1981) https://doi.org/10.1364/AO.20.003382
18. Birch K P and Downs M J 1993 Metrologia 30 155 https://doi.org/10.1088/0026- 1394/30/3/004
19. Birch K P and Downs M J 1994 Metrologia 31 315 https://doi.org/10.1088/0026-1394/31/4/006
20. Schödel R et al 2021 The new mise en pratique for the metre—a review of approaches for the practical realization of traceable length metrology from 10−11 m to 1013 m Metrologia 58 052002 (20pp) https://doi.org/10.1088/1681-7575/ac1456
21. Klapetek P, A Yacoot A, Grolich P, Valtr M and Nečas D 2017 Gwyscan: a library to support non-equidistant scanning probe microscope measurements Meas. Sci. Technol. 28 034015 (11pp) https://doi.org/10.1088/1361-6501/28/3/034015
22. Anemos Lab lab.anemos.co.uk